

NASA TECHNICAL NOTE



NASA TN D-4702

CI

NASA TN D-4702



LOAN COPY: RETURN TO
AFWL (WLIL-2)
KIRTLAND AFB, N MEX

**PREDICTION OF
FATIGUE-CRACK-PROPAGATION BEHAVIOR
IN PANELS WITH SIMULATED RIVET FORCES**

by I. E. Figge and J. C. Newman, Jr.

Langley Research Center

Langley Station, Hampton, Va.



NATIONAL AERONAUTICS AND SPACE ADMINISTRATION • WASHINGTON, D. C. • AUGUST 1968

ERRATA

NASA Technical Note D-4702

PREDICTION OF FATIGUE-CRACK-PROPAGATION BEHAVIOR IN PANELS WITH SIMULATED RIVET FORCES

By I. E. Figge and J. C. Newman, Jr.

August 1968

Page 8, equation (11): In the equation for I_2 , the numerator is incorrect because a plus sign was inadvertently left out after the bracket. The equation should read

$$I_2 = \frac{\left\{ y_o(1 + \eta) \left[(x_o - a_e)^2 + y_o^2 \right] + 2y_o a_e (x_o - a_e) \right\} \cos \left(\frac{1}{2} \tan^{-1} \frac{2x_o y_o}{x_o^2 - y_o^2 - a_e^2} \right)}{(1 + \eta) \left[(x_o - a_e)^2 + y_o^2 \right] \left[(x_o^2 - y_o^2 - a_e^2)^2 + 4x_o^2 y_o^2 \right]^{1/4}}$$



0131297

PREDICTION OF FATIGUE-CRACK-PROPAGATION BEHAVIOR
IN PANELS WITH SIMULATED RIVET FORCES

By I. E. Figge and J. C. Newman, Jr.

Langley Research Center
Langley Station, Hampton, Va.

NATIONAL AERONAUTICS AND SPACE ADMINISTRATION

For sale by the Clearinghouse for Federal Scientific and Technical Information
Springfield, Virginia 22151 - CFSTI price \$3.00

PREDICTION OF FATIGUE-CRACK-PROPAGATION BEHAVIOR IN PANELS WITH SIMULATED RIVET FORCES

By I. E. Figge and J. C. Newman, Jr.
Langley Research Center

SUMMARY

Analytical and experimental studies were conducted to determine the rates of fatigue-crack propagation in 7075-T6 aluminum-alloy sheet specimens containing either symmetric or nonsymmetric cracks subjected to uniform end loads, concentrated loads, or combinations of both. The concentrated loads simulated rivet forces and were applied by a special hydraulic fixture which is described.

These studies indicate that the curve of stress-intensity factor against crack growth rate obtained from tests on simple specimens of a given material tested at load ratios of 0.05 to -1 can be successfully used to predict the crack-propagation behavior of complex specimens of the same material tested over the same range of load ratios. It was also observed that better predictions of life were obtained for panels subjected to concentrated forces when the stress-intensity factors were obtained by using the measured strains on the uncracked panels rather than by using those obtained from the theoretical point load solutions.

INTRODUCTION

Various authors have shown that fatigue-crack-propagation behavior of simple specimens can be correlated with the stress state at the tip of the crack as defined by the stress-intensity factor. (See refs. 1 to 4.) The specimens used in references 1 to 3 were loaded by either uniform end loads or by concentrated forces applied to the crack surface. In reference 1 the authors stated "It is expected that such methods can be further developed to correlate all specimen behavior and all structural behavior for which analytical solutions or reasonable approximations are known or can be found." A similar hypothesis was stated in reference 2.

The purpose of the present investigation was to demonstrate that the relation between the rate of fatigue-crack propagation and the stress-intensity factor obtained from tests on simple specimens could be used to predict the crack-propagation behavior of specimens having configurations similar to those occurring in built-up structures.

This report is divided into two parts. The first part concerns itself with the specimens and techniques used to "characterize the material," that is, to obtain the relation between the stress-intensity factor and the crack growth rate. The second part of this report concerns itself with the analysis of five specimen configurations which approximate the geometry and loading conditions in built-up structures. The method of calculating the stress-intensity factor for each configuration is described and comparisons are made between the predicted and experimental results.

SYMBOLS

The units used for the physical quantities defined in this paper are given in U.S. Customary Units and in the International System of Units (SI) (ref. 5). Appendix A presents factors relating these two systems of units.

a	half-length of crack, inches (centimeters)
a_e	equivalent half-length of crack, inches (centimeters)
a_i	initial half-length of crack, inches (centimeters)
b	half-width of specimen, inches (centimeters)
D	pin diameter, inches (centimeters)
d	perpendicular distance from center line of specimen to center of hole, inches (centimeters)
da/dN	fatigue-crack growth rate, inches/cycle (meters/cycle)
e	distance from the center of a crack to the vertical center line of the specimen, inches (centimeters)
h	half-length of specimen, inches (centimeters)
k	stress-intensity factor, pound-inch ^{-3/2} (meganewton-meter ^{-3/2})
k_{max}	stress-intensity factor corresponding to maximum load, pound-inch ^{-3/2} (meganewton-meter ^{-3/2})
L	length of crack from one side of a hole, inches (centimeters)

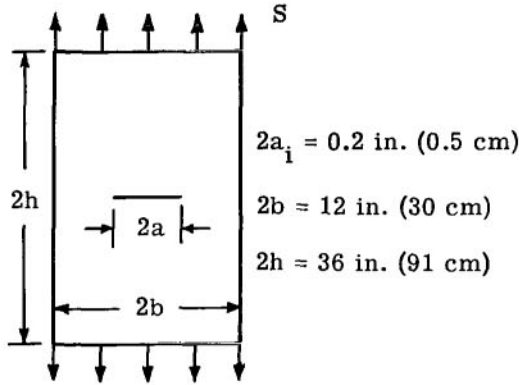
L_i	initial length of crack from one side of a hole, inches (meters)
N	number of load cycles
P	concentrated force, pounds (newtons)
P_{\max}	maximum concentrated force during cyclic loading, pounds (newtons)
P_{\min}	minimum concentrated force during cyclic loading, pounds (newtons)
R	load ratio, minimum load to maximum load
S	uniform stress applied to the ends of the panels (based on gross area), kilopounds/square inch (meganewtons/meter ²)
S_{\max}	maximum uniform stress during cyclic loading (based on gross area), kilopounds/square inch (meganewtons/meter ²)
t	plate thickness, inches (centimeters)
x_0	perpendicular distance from center line of crack to point of application of concentrated force, inches (centimeters)
y_0	perpendicular distance from plane of crack to point of application of con- centrated force (midpoint of bearing interface), inches (centimeters)
$\sigma(x)$	stress distribution in uncracked panel normal to the x-axis, kilopounds/square inch (meganewtons/meter ²)
ν	Poisson's ratio
ρ	radius of hole, inches (centimeters)

CHARACTERIZATION OF MATERIAL

As shown in references 1 to 3 the crack-propagation behavior of simple specimens from a given material can be characterized by plotting the stress-intensity factor against crack growth rate. The curve of stress-intensity factor (maximum during cycle) against crack growth rate, henceforth called the k-rate curve, was obtained for the 7075-T6 aluminum alloy studied in this investigation by using center-cracked specimens subjected

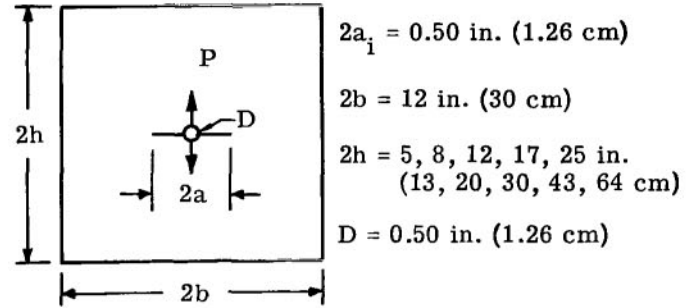
to either uniformly distributed end loads or to concentrated forces on the crack surface (hereafter called uniform load and wedge force, respectively). The ratio of minimum to maximum load for these tests was 0.05. The dimensions of the specimens are given in sketches (a) and (b).

Uniformly loaded panel



Sketch (a)

Wedge-force panel



Sketch (b)

Details of the equipment and test procedures used are presented in appendix B. The crack-propagation data obtained from these specimens are presented in table I. The stress-intensity factors for these specimens were obtained as follows:

The stress-intensity factor for a panel with uniform load was obtained from reference 6 and is

$$k = S \sqrt{a} F\left(\frac{a}{b}\right) \quad (1)$$

where $F\left(\frac{a}{b}\right)$ is a boundary-correction factor which adjusts the stress-intensity factor for an infinite plate to account for the influence of the finite width of the panel. The boundary-correction factor was obtained from the solution for the elastic-stress concentration at an elliptic hole in a strip of infinite length and finite width subjected to a uniform load. (See ref. 7.) The influence of specimen length $2h$ and grip constraint were assumed to be of minor importance when the length-width ratio was greater than 2.

The stress-intensity factor for the wedge force-loaded panel was obtained from reference 6 and is

$$k = \frac{P}{\pi t \sqrt{a}} F\left(\frac{a}{b}, \frac{a}{h}\right) \quad (2)$$

where $F\left(\frac{a}{b}, \frac{a}{h}\right)$ is a boundary-correction factor accounting for both finite width and length. The boundary-correction factor was approximated by superposing the solutions for a strip

of infinite length and finite width (ref. 6) and one of infinite width and finite length (ref. 8) and resulted in the following expression:

$$F\left(\frac{a}{b}, \frac{a}{h}\right) = \frac{G\left(\frac{a}{h}\right)}{\sqrt{\frac{b}{\pi a} \sin \frac{\pi a}{b}}} \quad (3)$$

where $G\left(\frac{a}{h}\right)$ was approximated by the following expression:

$$G\left(\frac{a}{h}\right) \approx 1 - 0.08\left(\frac{a}{h}\right) + 2.69\left(\frac{a}{h}\right)^2 - 0.91\left(\frac{a}{h}\right)^3 \quad (4)$$

With the foregoing expressions for k and the data from table I, the k -rate curve for the 7075-T6 alloy at a load ratio of 0.05 was calculated and is presented in figure 1. The solid and dashed curves represent the mean (logarithmic) and extremes of the experimental data, respectively. As in references 1 and 2, the data for both types of loading fell along the same curve. It should be noted that the k -rate curve presented in figure 1 is considered applicable for values of load ratio from 0.05 to -1 since it has been shown that the compressive portion of the load cycle does not contribute appreciably to the rate of crack growth in 7075-T6 aluminum alloy (refs. 1 and 9) and the differences in the range of zero to 0.05 are assumed to be negligible.

If it is assumed, as in references 1 and 2, that the curve in figure 1 truly characterizes the crack-propagation behavior of the material at the load ranges of interest, the curve can be used as the basic tool for making predictions of the crack-propagation behavior of more complex configurations. Predictions of crack length against the number of cycles are obtained by calculating the variation in the stress-intensity factor as the crack advances and then using this information to integrate numerically the k -rate curve in figure 1.

In the following sections, analytical expressions for the stress-intensity factor for five configurations are presented. The experimentally determined crack-propagation behavior is compared with predictions based on the k -rate curve of figure 1.

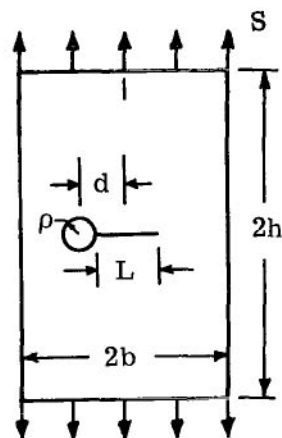
ANALYSIS AND EXPERIMENTAL RESULTS FOR PANELS SUBJECTED TO VARIOUS COMBINATIONS OF LOAD

In the following section, the analysis of each configuration used is described in detail. In general, theoretical stress-intensity solutions obtained from the literature were used. Superposition of these solutions was used where appropriate. Comparisons are made between the experimental and predicted curves of crack length against cycles

for each configuration. The prediction of crack length against cycles was based on the logarithmic mean and the extremes of the crack-growth-rate data in figure 1. The experimental crack-propagation data are presented in table I.

Case A

For the growth of a fatigue crack from one side of a hole located eccentrically in a uniformly loaded panel (sketch (c)), the assumption was made that the combination of crack and hole could be represented by an equivalent crack. Thereby, the problem of an eccentric hole and single crack is reduced to the case of an eccentric crack in a panel. The reason for using an equivalent crack was that finite boundary corrections did not exist in the literature for the case of an eccentric



Sketch (c)

$$\begin{aligned} L_i &= 0.15 \text{ in. (0.38 cm)} \\ 2b &= 12 \text{ in. (30 cm)} \\ 2h &= 36 \text{ in. (91 cm)} \\ d &= 3.0 \text{ in. (7.6 cm)} \\ \rho &= 0.50 \text{ in. (1.26 cm)} \end{aligned}$$

hole and crack, but did exist for the case of an eccentric crack in a panel. The equivalent crack length was obtained by equating the stress-intensity factors for an infinite plate containing a hole and single crack with that for an infinite plate with a crack. The stress intensities were obtained from references 10 and 6, and are, respectively,

$$k = S\sqrt{L} F\left(\frac{L}{\rho}\right) \quad (5)$$

and

$$k = S\sqrt{a_e} \quad (6)$$

where $F\left(\frac{L}{\rho}\right)$ is a function which describes the influence of the hole on the stress-intensity factor. Eliminating k with the use of equations (5) and (6) and solving for a_e results in the relation for the equivalent crack length

$$a_e = L \left[F\left(\frac{L}{\rho}\right) \right]^2 \quad (7)$$

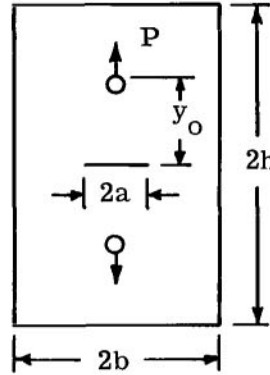
The equivalent crack length calculated by equation (7) is very nearly equal to the sum of the actual crack length plus hole diameter. The stress-intensity factor for case A is then

$$k = S\sqrt{a_e} F\left(\frac{e}{b}, \frac{a_e}{b}\right) \quad (8)$$

where $F\left(\frac{e}{b}, \frac{a}{b}\right)$ is the boundary-correction factor which accounts for the crack eccentricity and finite width. (See ref. 11.) The predicted mean and the possible scatter in data for crack length plotted against cycles are presented in figure 2 as a solid line and shaded area, respectively. The symbols represent the data obtained from two identical tests and show good agreement with the predicted results.

Case B

The simulation of rivet forces in the testing laboratory is important to the understanding of the parameters which influence fatigue-crack growth in the vicinity of rivets in structures. The growth of a symmetrical fatigue crack in a panel loaded with concentrated forces (sketch (d)) simulated the growth of a fatigue crack in a riveted doubler. Cyclic loads were applied by two pins located along the longitudinal center line of the panel. In this case, the stress-intensity equation for loads applied at a point was assumed to be applicable since the pins were located more than 5 diameters away from the plane of the crack. The stress-intensity factor for a crack in an infinite plate with symmetric point loads was obtained from reference 12. The solution for a finite panel is



$$\begin{aligned} 2a_i &= 1.0 \text{ in. (2.5 cm)} \\ 2b &= 12 \text{ in. (30 cm)} \\ 2h &= 12 \text{ in. (30 cm)} \\ y_o &= 2.25 \text{ in. (5.7 cm)} \\ D &= 0.38 \text{ in. (0.96 cm)} \end{aligned}$$

Sketch (d)

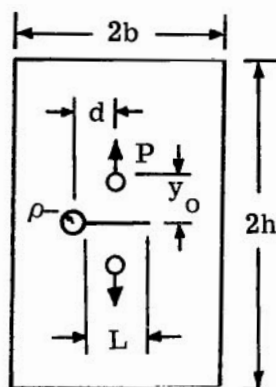
$$k = \frac{P\sqrt{a}}{2\pi t} \left[\frac{(3 + \nu)y_o^2 + 2a^2}{(a^2 + y_o^2)^{3/2}} \right] F\left(\frac{a}{b}, \frac{a}{h}\right) \quad (9)$$

where $F\left(\frac{a}{b}, \frac{a}{h}\right)$ is an approximate boundary-correction factor. (See eq. (3).)

The prediction of the crack-length-against-cycles curve for this specimen is shown in figure 3. As in case A, the predicted mean and the possible scatter in the data for crack length plotted against cycles are presented as a solid line and shaded area, respectively. The symbols represent the data obtained from tests of two identical specimens and show reasonable agreement with the predicted results.

The growth of a fatigue crack from one side of a hole located eccentrically in a panel subjected to concentrated forces (sketch (e)) is designated case C. Case C is similar to case A, except that the loading was by concentrated forces. The theoretical stress-intensity factor for a crack which is eccentric with respect to the line of load application in an infinite plate subjected to concentrated forces was obtained from reference 13. This solution was adjusted by using the equivalent crack length as in case A. The stress intensity for case C is:

Case C



Sketch (e)

$$\begin{aligned} L_i &= 0.8 \text{ in. (2 cm)} \\ 2b &= 12 \text{ in. (30 cm)} \\ 2h &= 12 \text{ in. (30 cm)} \\ y_o &= 0.91 \text{ in. (2.3 cm)} \\ \rho &= 0.18 \text{ in. (0.45 cm)} \\ d &= 1.45 \text{ in. (3.68 cm)} \\ D &= 0.50 \text{ in. (1.26 cm)} \end{aligned}$$

$$k = \frac{P}{\pi t \sqrt{a_e}} (I_1 - I_2) F\left(\frac{a_e}{b}, \frac{a_e}{h}\right) \quad (10)$$

The quantities I_1 and I_2 are given by:

$$\left. \begin{aligned} I_1 &= \frac{\left\{ (a_e + x_o)(1 + \eta) \left[(x_o - a_e)^2 + y_o^2 \right] + 2y_o^2 a_e \right\} \sin\left(\frac{1}{2} \tan^{-1} \frac{2x_o y_o}{x_o^2 - y_o^2 - a_e^2}\right)}{(1 + \eta) \left[(x_o - a_e)^2 + y_o^2 \right] \left[(x_o^2 - y_o^2 - a_e^2)^2 + 4x_o^2 y_o^2 \right]^{1/4}} \\ I_2 &= \frac{\left\{ y_o(1 + \eta) \left[(x_o - a_e)^2 + y_o^2 \right] 2y_o a_e (x_o - a_e) \right\} \cos\left(\frac{1}{2} \tan^{-1} \frac{2x_o y_o}{x_o^2 - y_o^2 - a_e^2}\right)}{(1 + \eta) \left[(x_o - a_e)^2 + y_o^2 \right] \left[(x_o^2 - y_o^2 - a_e^2)^2 + 4x_o^2 y_o^2 \right]^{1/4}} \end{aligned} \right\} \quad (11)$$

See equation

where

$$\eta = \frac{3 - \nu}{1 + \nu}$$

The boundary-correction factor accounting for crack eccentricity was negligible for this case.

Equation (10) assumes theoretical point loading. However, in this case, the pins were located reasonably close to the plane of the crack and thus the finite pin size was expected to influence the crack growth. In order to determine the actual stress distribution on the panel resulting from the pin loading, strain gages were placed along the transverse axis of an uncracked panel and strains were measured at the loads of interest. The stress distribution obtained from the strain readings is presented in figure 4. Also presented in the figure is the theoretical solution which assumes point loadings. (See ref. 14.) Opposite trends in the stress distribution were found in the region between the pins for a distance approximately equal to the pin diameter. Since noticeable differences were observed, a stress-intensity factor which takes into account the actual stress distribution on the uncracked panel was calculated by using the following stress-intensity equation for an infinite sheet (from ref. 12):

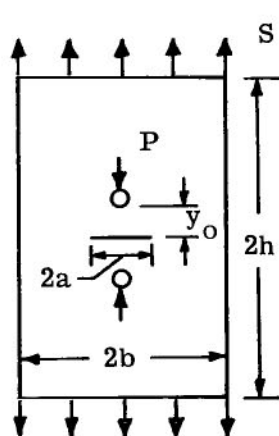
$$k = \frac{1}{\pi \sqrt{a}} \int_{-a}^a \sigma(x) \sqrt{\frac{a+x}{a-x}} dx \quad (12)$$

where $\sigma(x)$ was calculated from strain readings obtained from the uncracked panel subjected to the maximum load conditions expected during the cyclic testing. Numerical integration of this expression yielded the stress-intensity factor as a function of crack length.

The predictions based on equation (10) and on equation (12) for crack length plotted against cycles are shown in figure 5 as solid and dashed curves, respectively. The curve obtained from equation (12) approaches the trend of the data and produces substantially better agreement with experiment than the results obtained from equation (10).

Case D

The specimens for growth of a symmetrical fatigue crack in a panel subjected to uniform load and concentrated forces (sketch (f)) are of particular interest because of the similarity to the actual case of a crack propagating in the skin material of an aircraft under a riveted stiffener. A series of specimens were investigated in this case. The parameters studied included pin spacing, pin diameter, and load. The pin loadings (simulated rivets) were applied by a hydraulic jack under steady pressure (constant load). The forces on



Sketch (f)

$2a_i$	= 1.0 in. (2.5 cm)
$2b$	= 8 in. (20 cm)
$2h$	= 24 in. (61 cm)
y_o	= 0.50 in. (1.26 cm)
	0.75 in. (1.90 cm)
	1.00 in. (2.54 cm)
	1.50 in. (3.81 cm)
	2.00 in. (5.08 cm)
D	= 0.25 in. (0.63 cm)
	= 0.50 in. (1.26 cm)

the pins fluctuated slightly as a result of the cyclic uniform loading, but at all times tended to close the crack. The stress at the tip of the crack thus varied between tension and compression. However, the k-rate curve for a load ratio of 0.05 was considered applicable. (See section "Characterization of Material.")

The theoretical stress intensity factor for this case was obtained by superposing the stress-intensity factors for a centrally cracked panel subjected to uniform load (refs. 6 and 7) and that for a centrally cracked panel subjected to concentrated forces (ref. 12). These solutions were adjusted to account for finite width (see ref. 6) and are, respectively,

$$k = S\sqrt{a} F\left(\frac{a}{b}\right) \quad (13)$$

and

$$k = \frac{P\sqrt{a}}{2\pi t} \left[\frac{(3 + \nu)y_0^2 + 2a^2}{(a^2 + y_0^2)^{3/2}} \right] F\left(\frac{a}{b}\right) \quad (14)$$

Inasmuch as the concentrated forces tended to close the crack, it was necessary to use equation (14) with a negative sign to account for the direction of loading. A schematic representation of these two solutions and their algebraic sum are represented in figure 6.

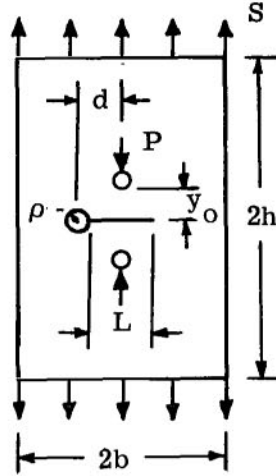
As in case C, the finite size of the pin hole was expected to influence the stress distribution. The combined influence of the jack-mounting hole (see appendix B) and pin holes on the stress distribution along the transverse axis on a panel subjected to uniform loading is presented in figure 7(a). The influence of finite pin size on the stress distribution of a panel subjected to concentrated forces is presented in figure 7(b). Also shown in the figures are the theoretical stress distributions obtained by using the solutions for point loads. Noticeable differences between the theoretical and measured stress distribution along the X-axis were observed in the vicinity of the pin holes.

The experimental results and the predictions obtained by using the resultant theoretical stress-intensity expression and those obtained by using equation (12) are presented in figures 8(a) and 8(b). Predictions were made by using equation (12) only for those specimens with y_0 equal to 1.0 inch (2.54 cm) since they were the only specimens for which the measured strain distributions were obtained. For the specimens loaded with high values of concentrated force, it was necessary to allow the fatigue crack to propagate to a total length of approximately 1 inch (2.54 cm) prior to applying the concentrated force. This procedure was followed in order to prevent cracks from starting in the vicinity of the pin holes. For consistency, all the crack-length data presented in figure 8 start at a length of 1.2 inches (3.05 cm). As expected, high pin forces or small pin spacings retarded crack growth. The largest pin force used in the study increased the life by about a factor of 7 over that obtained when the pin force was zero. In general,

the predictions obtained by using equation (12) were very good and produced substantially better agreement with the data than those based on theoretical point load.

Case E

The growth of a fatigue crack from one side of a hole located eccentrically in a panel subjected to a uniform load and concentrated forces is designated case E (sketch (g)). Case E is similar to cases A and C and represents a fatigue crack propagating from one side of an eccentric hole toward a row of rivets in a stiffened panel. The concentrated forces were applied in the same manner as in case D. Again, both theoretical-stress intensities and those based on strain-gage measurements (eq. (12)) were used in the predictions.



- $L_i = 0.2$ in. (0.5 cm)
- $2b = 12$ in. (30 cm)
- $2h = 36$ in. (91 cm)
- $y_o = 1.0$ in. (2.5 cm)
- $\rho = 0.50$ in. (1.26 cm)
- $d = 3.0$ in. (7.6 cm)
- $D = 0.50$ in. (1.26 cm)

Sketch (g)

The resultant theoretical stress-intensity factor for this case was obtained by superposition of the stress intensity for a centrally cracked panel subjected to uniform load and that for the concentrated forces. The stress-intensity factor for a single crack growing from one side of an eccentric hole in a panel subjected to uniform load was obtained by using the equivalent crack length a_e as in case A, and is

$$k = S\sqrt{a_e} F\left(\frac{e}{b}, \frac{a_e}{b}\right) \quad (15)$$

The stress-intensity factor for concentrated forces applied to the same configuration is

$$k = \frac{P}{\pi t \sqrt{a_e}} (I_1 - I_2) F\left(\frac{e}{b}, \frac{a_e}{b}\right) \quad (16)$$

A boundary-correction factor was not available for this loading configuration. However, it was assumed that the correction factor applied to the uniformly loaded panel would give reasonable results. The quantities I_1 and I_2 are defined in case C. Since the concentrated forces tended to close the crack, the stress-intensity factor for the concentrated forces (eq. (16)) was used with a negative sign. The algebraic sum of the stress intensities for these two cases is represented in figure 9. As in case D, the k -rate curve for a load ratio of 0.05 was considered applicable. The predicted curves of crack length against cycles for this specimen are shown in figure 10, together with the data obtained from one test. The agreement between the actual cycles and those predicted by using the

resultant stress-intensity solution (solid curve) was considered good except when the crack tip was located to the right of the line of action of the pin forces. This disagreement was attributed to the reduction in stress along the plane of the crack due to the finite pin size in a manner similar to that encountered in cases C and D. The predictions based on equation (12) (dashed curve) gave substantially better agreement with the data in the region where the crack extended beyond the line of action of the pin forces.

CONCLUDING REMARKS

Analytical and experimental studies were conducted on the rates of fatigue-crack propagation in 7075-T6 aluminum-alloy sheet specimens subjected to combinations of uniform load and concentrated forces similar to those occurring in built-up structures. These studies indicate that the curve of stress-intensity factor plotted against crack-growth rate obtained from tests on simple specimens of a given material tested at load ratios of 0.05 to -1 can be successfully used to predict the crack-propagation behavior of complex specimens of the same material tested over the same range of load ratios. It was also observed that better predictions of life were obtained for panels subjected to concentrated forces when the stress-intensity factors were obtained by using measured strains on the uncracked panels rather than by using those obtained from theoretical point load solutions.

Langley Research Center,
National Aeronautics and Space Administration,
Langley Station, Hampton, Va., April 16, 1968,
126-14-03-01-23.

APPENDIX A

CONVERSION OF U.S. CUSTOMARY UNITS TO SI UNITS

The International System of Units (SI) was adopted by the Eleventh General Conference of Weights and Measures, Paris, October 1960, in Resolution No. 12 (ref. 5). Conversion factors for the units used herein are given in the following table:

Physical quantity	U.S. Customary Unit	Conversion factor (*)	SI Unit
Force	lbf	4.448222	newton (N)
Length	in.	2.54×10^{-2}	meter (m)
Stress	ksi	6.894757	meganewton/meter ² (MN/m ²)
Stress-intensity factor . . .	lbf-in ^{-3/2}	1.099×10^{-3}	MN-m ^{-3/2}
Frequency	cpm	1.67×10^{-2}	hertz (Hz)

*Multiply value given in U.S. Customary Unit by conversion factor to obtain equivalent value in SI Unit.

Prefixes to indicate multiple of units are as follows:

Prefix	Multiple
micro (μ)	10^{-6}
milli (m)	10^{-3}
centi (c)	10^{-2}
kilo (k)	10^3
mega (M)	10^6

APPENDIX B

SPECIMENS, EQUIPMENT, AND TEST PROCEDURES

The panels studied were constructed of 0.090-in. (2.28 mm) thick 7075-T6 aluminum alloy. The material was obtained from a special fatigue stock (see ref. 15) retained at Langley Research Center for fatigue testing. A slit perpendicular to the direction of loading was produced in each specimen by either a saw cut or by a spark-discharge technique to act as a crack starter. A grid was photographically printed on each specimen to facilitate measurement of crack growth. The line spacing in the grid was 0.05 inch (1.27 mm). Both metallographic and tensile tests revealed that the grid had no detrimental effect on the material. In order to follow the crack growth, the fatigue cracks were observed through a 30-power microscope while illuminated by stroboscopic light.

The axial-load fatigue testing equipment used in this investigation included a subresonant machine (ref. 16), an inertia-force compensating machine, and a combination hydraulic and subresonant machine (ref. 16). The subresonant machine had an operating frequency of 1800 cpm (30 Hz) and a load capacity of $\pm 20\,000$ pounds (89 kN). The inertia-force compensating machine had an operating frequency of 1200 cpm (20 Hz) and a load capacity of $\pm 20\,000$ pounds (89 kN). The combination hydraulic and subresonant machine was operated only in the hydraulic mode. In this mode the operating frequency was 50 cpm (0.8 Hz) and the load capacity was 132 000 pounds (586 kN).

Two types of specially designed fixtures (fig. 11) were used in this investigation to apply concentrated cyclic tension forces to the test specimens. The type shown in figure 11(a) was used for the cases in which the pin holes were remote from the crack whereas the type shown in figure 11(b) was used to apply loads as near to the crack surface as possible. In the latter case, the pins were semicircular in cross section and two were inserted in the same hole.

The type of fixture used to apply concentrated compressive forces is shown schematically in figure 12. The fixture consisted of a small hydraulic jack and sets of straps which transmitted the loads through pins to the specimen. The outer straps were attached to the jack ram by a pin which passed through slots in the inner straps. The inner straps were attached to the cylinder of the jack. The inner and outer straps were in the same plane. Two observation slots were provided in the legs of the outer straps to permit observations of the crack as it grew under the legs. Strain gages were mounted on each leg of the outer straps to monitor loads. The jack was mounted in a hole in the specimen located approximately $6\frac{1}{2}$ inches (16.5 cm) from the plane of the crack. The center of the jack was on the center line of the specimen in both the width and thickness directions. Pressure was applied to the jack by an accumulator and was set at the desired value prior

APPENDIX B

to application of the uniform cyclic loads. The pressure, and thus the concentrated load, fluctuated approximately ± 8 percent as the specimen was cycled. The minimum and maximum compressive forces on the specimen occurred when the uniform cyclic forces were a minimum and maximum, respectively.

REFERENCES

1. Donaldson, D. R.; and Anderson, W. E.: Crack Propagation Behavior of Some Air-frame Materials. Paper presented at Crack Propagation Symposium (Cranfield, England), Sept. 1961.
2. Paris, Paul C.: The Fracture Mechanics Approach to Fatigue. Fatigue - An Interdisciplinary Approach, John J. Burke, Norman L. Reed, and Volker Weiss, eds., Syracuse Univ. Press, 1964, pp. 107-132.
3. Hudson, C. Michael; and Scardina, Joseph T.: Effect of Stress Ratio on Fatigue-Crack Growth in 7075-T6 Aluminum-Alloy Sheet. National Symposium on Fracture Mechanics, June 1967.
4. Figge, I. E.; and Newman, J. C., Jr.: Fatigue Crack Propagation in Structures With Simulated Rivet Forces. Spec. Tech. Publ. No. 415, Amer. Soc. Testing Mater., c.1967, pp. 71-94.
5. Comm. on Metric Pract.: ASTM Metric Practice Guide. NBS Handbook 102, U.S. Dep. Com., Mar. 10, 1967.
6. Paris, Paul C.; and Sih, George C.: Stress Analysis of Cracks. Fracture Toughness Testing and Its Applications, Spec. Tech. Publ. No. 381, Am. Soc. Testing Mater., c.1965, pp. 30-83.
7. Isida, M.: On the Tension of a Strip With a Central Elliptical Hole. Trans. Japan Soc. Mech. Engrs., vol. 21, no. 107, 1955, p. 511.
8. Fichter, W. B.: Effects of Strip Width on Stress at the Tip of a Longitudinal Crack in a Plate Strip. Paper presented at Fifth U.S. National Congress of Applied Mechanics (Minneapolis, Minn.), June 1966.
9. Ilg, Walter; and McEvily, Arthur J., Jr.: The Rate of Fatigue-Crack Propagation for Two Aluminum Alloys Under Completely Reversed Loading. NASA TN D-52, 1959.
10. Bowie, O. L.: Analysis of an Infinite Plate Containing Radial Cracks Originating From a Circular Hole. Jour. Math. Phys., vol. XXXV, no. 1, Apr. 1956, pp. 60-71.
11. Isida, M.: Crack Tip Stress Intensity Factors for the Tensions of an Eccentrically Cracked Strip. Dept. Mech., Lehigh Univ., Sept. 1965.
12. Paris, Paul C.: Application of Muskhelishvili's Methods to the Analysis of Crack Tip Stress Intensity Factors for Plane Problems. Pt. III. Inst. Research, Lehigh Univ., June 1960.
13. Erdogan, Fazil: The Stress Distribution in an Infinite Plate With Two Co-Linear Cracks Subjected to Arbitrary Loads in Its Plane. Inst. Research, Lehigh Univ., June 1961.

14. Timoshenko, S.; and Goodier, J. N.: Theory of Elasticity. Second ed., McGraw-Hill Book Co., Inc., 1951.
15. Grover, H. J.; Hyler, W. S.; Kuhn, Paul; Landers, Charles B.; and Howell, F. M.: Axial-Load Fatigue Properties of 24S-T and 75S-T Aluminum Alloy as Determined in Several Laboratories. NACA Rep. 1190, 1954. (Supersedes NACA TN 2928.)
16. Hudson, C. Michael; and Hardrath, Herbert F.: Investigation of the Effects of Variable-Amplitude Loadings on Fatigue Crack Propagation Patterns. NASA TN D-1803, 1963.

TABLE I.- FATIGUE-CRACK-PROPAGATION DATA FOR 7075-T6 ALUMINUM ALLOY AT $R = 0.05$ $[t = 0.90 \text{ in. (0.23 cm)}]$ (a) Uniformly loaded panel. $2b = 12 \text{ in. (30 cm)}$; $2h = 36 \text{ in. (91 cm)}$

S		Number of kilocycles required to propagate a crack from a total length of 0.60 in. (1.52 cm) to a length of -															
ksi	MN/m ²	0.8 in. (2.03 cm)	1.0 in. (2.54 cm)	1.2 in. (3.05 cm)	1.4 in. (3.56 cm)	1.6 in. (4.06 cm)	1.8 in. (4.57 cm)	2.0 in. (5.08 cm)	2.2 in. (5.59 cm)	2.4 in. (6.10 cm)	2.6 in. (6.60 cm)	2.8 in. (7.11 cm)	3.0 in. (7.62 cm)	3.2 in. (8.13 cm)	3.4 in. (8.64 cm)	3.6 in. (9.14 cm)	3.8 in. (9.65 cm)
5.2	35.8	220	345	390	418	439	456	471	481	492	500	507	513	520	525	530	534
5.5	37.9	164	244	286	316	340	360	376	390	401	411	418	425	431	437	443	449

(b) Wedge-force panel. $2b = 12 \text{ in. (30 cm)}$

P		2h	Number of kilocycles required to propagate a crack from a total length of 1.0 in. (2.54 cm) to a length of -															
lbf	kN	in.	cm	1.2 in. (3.05 cm)	1.4 in. (3.56 cm)	1.6 in. (4.06 cm)	1.8 in. (4.57 cm)	2.0 in. (5.08 cm)	2.2 in. (5.59 cm)	2.4 in. (6.10 cm)	2.6 in. (6.60 cm)	2.8 in. (7.11 cm)	3.0 in. (7.62 cm)	3.2 in. (8.13 cm)	3.4 in. (8.64 cm)	3.6 in. (9.14 cm)	3.8 in. (9.65 cm)	4.0 in. (10.16 cm)
1000	4.44	25	64	14.8	35.3	59.7	87.3	127.3	176.5	232.5	317.5	475	685	915	1193	1523	1916	----
2000	8.89	17	43	4	8	14	20	27.5	37.5	48	60	74.5	90	108	128	142	164	182
1150	5.11	17	43	17	38	82	131	172	215	275	341	418	516	616	713	835	990	1148
2000	8.89	12	30	3	5	9	13	18	22	27	32	38	43	49	55	62	70	77
2000	8.89	12	30	2	4	7	11	15	20	25	31	37	43	50	57	64	73	79
2000	8.89	8	20	4	8	13	20	26	33	40	47	53	60	67	73	79	85	92
1150	5.11	8	20	12	26	42	64	94	137	187	236	289	311	342	370	404	433	461
2000	8.89	5	13	3	6	9	12	16	20	22	26	30	34	37	40	44	46	49
1150	5.11	5	13	12	24	37	50	64	77	90	102	114	126	137	148	157	167	177

(c) Case A. $S = 3.66 \text{ ksi (25.2 MN/m}^2\text{)}$; $2b = 12 \text{ in. (30 cm)}$; $2h = 36 \text{ in. (91 cm)}$

Specimen	Number of kilocycles required to propagate a crack from total length of 0.15 in. (0.38 cm) to a length of -																	
	0.35 in. (0.89 cm)	0.55 in. (1.40 cm)	0.75 in. (1.91 cm)	0.95 in. (2.41 cm)	1.15 in. (2.92 cm)	1.35 in. (3.43 cm)	1.55 in. (3.94 cm)	1.75 in. (4.45 cm)	2.15 in. (5.46 cm)	2.35 in. (5.97 cm)	2.55 in. (6.48 cm)	2.75 in. (6.99 cm)	3.15 in. (8.00 cm)	3.35 in. (8.51 cm)	3.55 in. (9.02 cm)	3.75 in. (9.53 cm)	3.95 in. (10.03 cm)	4.35 in. (11.05 cm)
1	314	512	660	768	877	953	1016	1073	1162	1199	1234	1270	1332	1356	1374	1393	1410	1439
2	302	508	649	765	864	940	1012	1070	1172	1219	1258	1296	1362	1393	1420	1444	1468	1510

(d) Case B. $P_{\max} = 1920 \text{ lbf (8.55 kN)}$; $2b = 12 \text{ in. (30 cm)}$; $2h = 12 \text{ in. (30 cm)}$

Specimen	Number of kilocycles required to propagate a crack from total length of 1.00 in. (2.54 cm) to a length of -														
	1.20 in. (3.05 cm)	1.40 in. (3.56 cm)	1.60 in. (4.06 cm)	1.80 in. (4.57 cm)	2.00 in. (5.08 cm)	2.20 in. (5.59 cm)	2.40 in. (6.10 cm)	2.60 in. (6.60 cm)	2.80 in. (7.11 cm)	3.00 in. (7.62 cm)	3.20 in. (8.13 cm)	3.40 in. (8.64 cm)	3.60 in. (9.14 cm)	3.80 in. (9.65 cm)	4.00 in. (10.16 cm)
1	27.1	50.8	68.8	84.9	99.8	115	123	135.5	144.2	154.3	163.8	172.6	182.2	191	198.4
2	40.6	68.6	91.4	111.6	129.4	141.8	157.8	176.8	187.6	196.3	207.9	221	230.8	242.5	----

(e) Case C. $P_{\max} = 1150 \text{ lbf (5.12 kN)}$; $2b = 12 \text{ in. (30 cm)}$; $2h = 12 \text{ in. (30 cm)}$

Specimen	Number of kilocycles required to propagate a crack from total length of 1.00 in. (2.54 cm) for specimen 1 and 0.80 in. (2.03 cm) for specimen 2 to a length of -										
	1.00 in. (2.54 cm)	1.20 in. (3.05 cm)	1.40 in. (3.56 cm)	1.60 in. (4.06 cm)	1.80 in. (4.57 cm)	2.00 in. (5.08 cm)	2.20 in. (5.59 cm)	2.40 in. (6.10 cm)	2.60 in. (6.60 cm)	2.80 in. (7.11 cm)	3.00 in. (7.62 cm)
1	---	94	216	408	488	540	589	636	697	771	846
2	93.4	170	345	500	579	621	668	719	772	835	917

TABLE I.- FATIGUE-CRACK-PROPAGATION DATA FOR 7075-T6 ALUMINUM ALLOY AT $R = 0.05$ - Concluded

(f) Case D. Pin diameter, 0.25 in. (0.63 cm); $S_{max} = 14.8$ ksi (102 MN/m²); $2b = 8$ in. (20 cm); $2h = 24$ in. (61 cm)

P		y_0		Number of kilocycles required to propagate a crack from total length of 1.20 in. (3.05 cm) to a length of -					
lbf	kN	in.	cm	1.40 in. (3.56 cm)	1.60 in. (4.06 cm)	1.80 in. (4.57 cm)	2.00 in. (5.08 cm)	2.20 in. (5.59 cm)	2.40 in. (6.10 cm)
0	0	1.00	2.54	1	1.75	2	2.75	3	3.25
485	2.16	1.00	2.54	3.9	6.95	8.9	10.8	----	----
735	3.27	.50	1.27	5.10	8.65	11.65	14.6	15.75	----
735	3.27	1.00	2.54	3.65	6.3	8.3	9.5	----	----
960	4.27	1.00	2.54	4.4	8.35	11.3	13.6	----	----
975	4.34	1.00	2.54	4.55	7.2	9.9	12	13.5	14.85
1125	5.00	.75	1.90	7.7	12.95	17.5	20.8	----	----
1185	5.27	1.00	2.54	6.65	11	14.95	17.5	----	----
1340	5.96	1.00	2.54	9.5	15.65	21.2	24.95	----	----
710	3.16	.50	1.27	6.95	11	14.25	16.9	----	----
735	3.27	1.00	2.54	5.25	9.65	13.25	15.5	17	18.1
765	3.40	.75	1.90	4.15	7.25	10	11.75	13.05	14.05
880	3.91	1.00	2.54	6.1	11.35	16.6	19.25	21.6	----
940	4.18	1.00	2.54	6.2	9.25	12.75	14.65	17	18.55
1140	5.07	1.00	2.54	11.15	17.05	21.05	25.25	27.75	----
1140	5.07	1.00	2.54	6.2	10.55	14.6	16.2	18.8	----
1200	5.34	1.00	2.54	10	14.35	18	20.9	22.7	24.3
1210	5.38	1.50	3.81	5.45	9.5	12.9	15.85	18	----
1210	5.38	2.00	5.08	4.05	7.25	9.55	11.75	13.5	----
1320	5.87	1.00	2.54	10.55	17.8	23.2	26.9	29.65	----

(g) Case E. $S_{max} = 8$ ksi (55.2 MN/m²); $P_{max} = 1090$ lbf (4.85 kN); $2b = 12$ in. (30 cm); $2h = 36$ in. (91 cm)

Specimen	Number of kilocycles required to propagate a crack from total length of 0.20 in. (0.51 cm) to a length of -															
	0.60 in. (1.52 cm)	1.00 in. (2.54 cm)	1.48 in. (3.76 cm)	2.00 in. (5.08 cm)	2.42 in. (6.15 cm)	2.62 in. (6.65 cm)	2.80 in. (7.11 cm)	2.98 in. (7.57 cm)	3.02 in. (7.65 cm)	3.12 in. (7.92 cm)	3.25 in. (8.25 cm)	3.55 in. (9.00 cm)	3.93 in. (9.98 cm)	4.45 in. (11.30 cm)	5.00 in. (12.70 cm)	5.50 in. (13.97 cm)
1	25	45	63	82	110	135	165	200	234	266	300	342	368	388	400	405

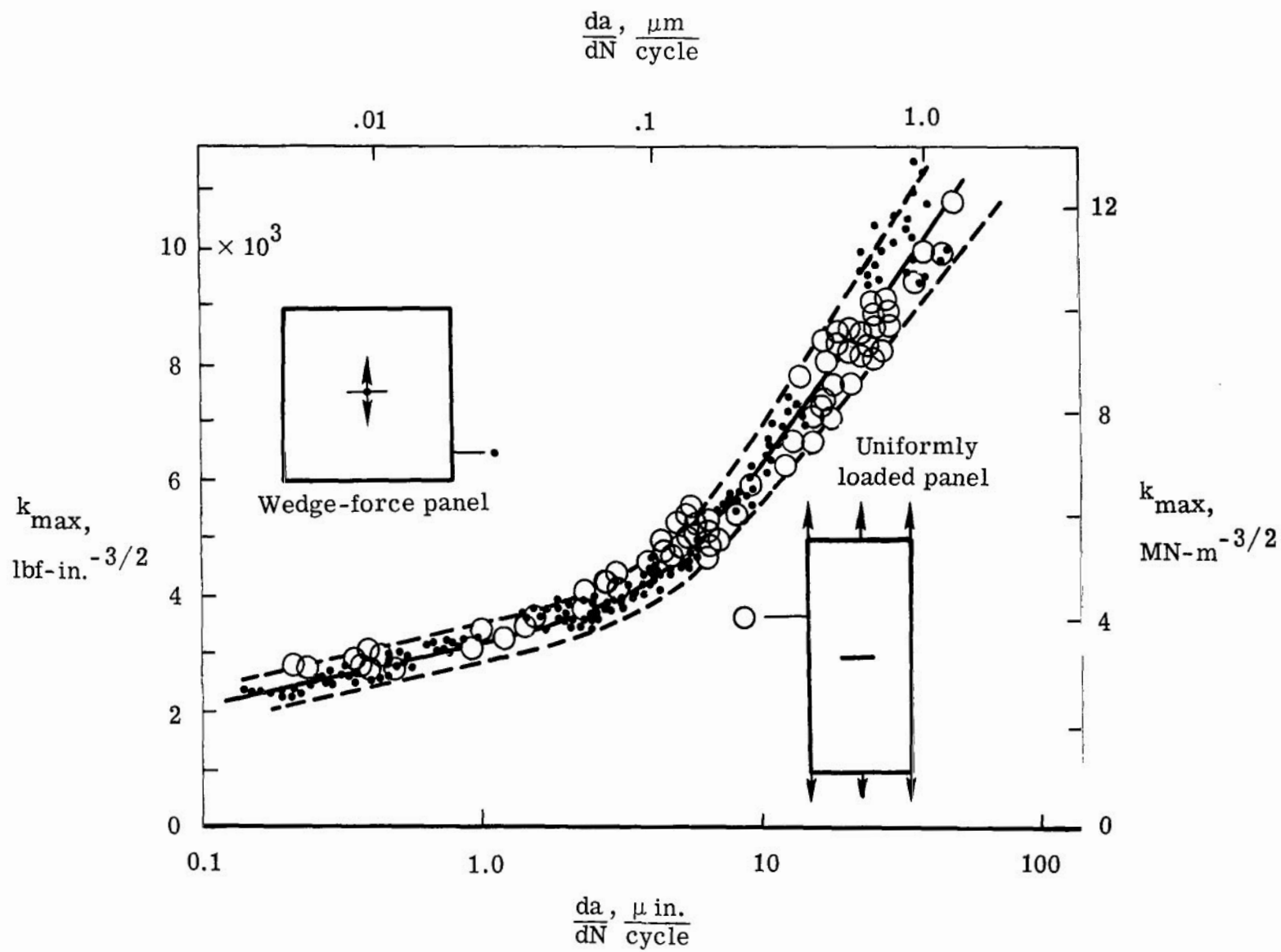


Figure 1.- Variation of stress-intensity factor with crack-growth rate for uniformly loaded and wedge force 7075-T6 aluminum-alloy panels at $R = 0.05$.

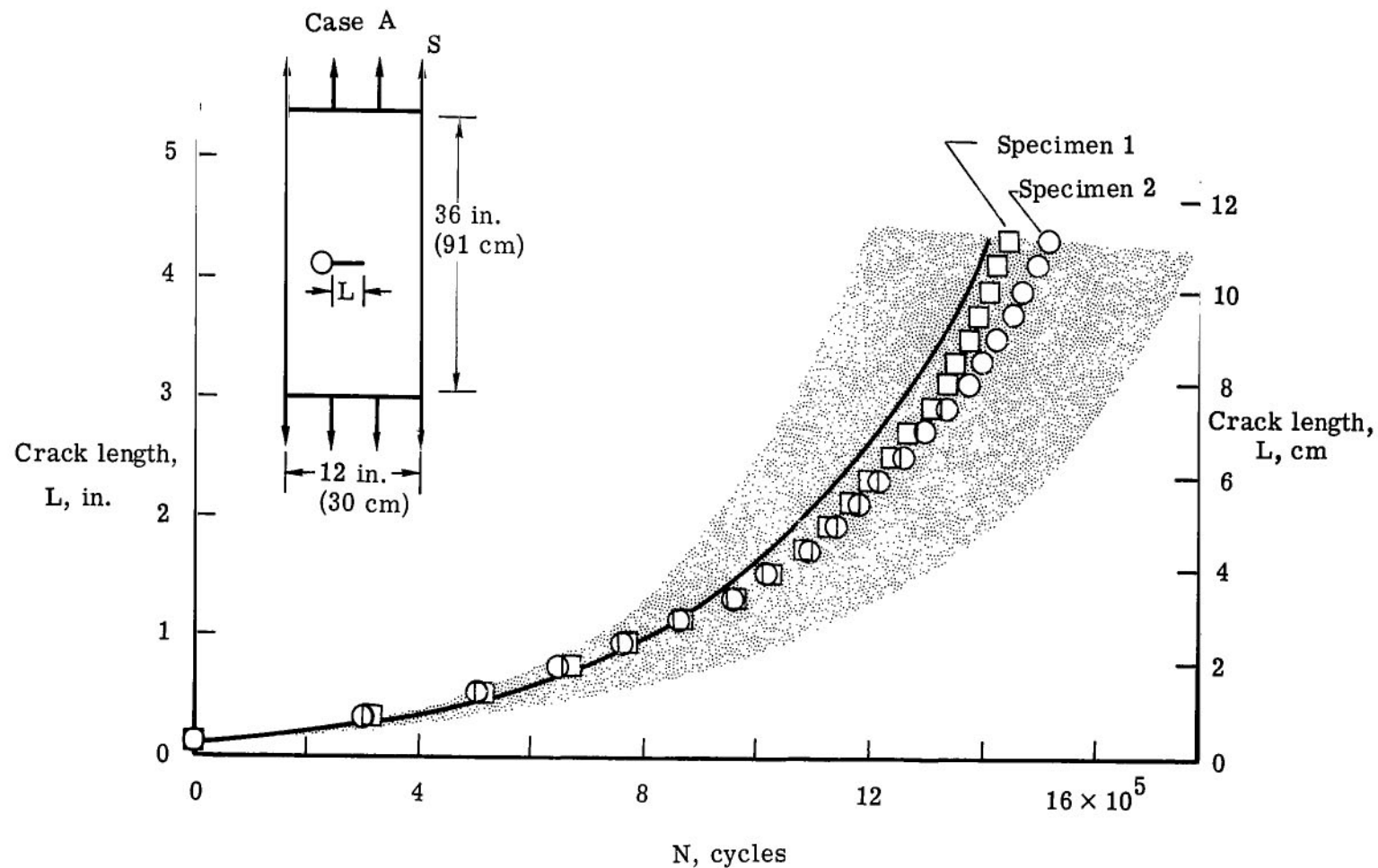


Figure 2.- Comparison of predicted and experimental fatigue crack propagation from one side of a hole located eccentrically in a uniformly loaded 7075-T6 aluminum-alloy panel. $S = 3.66$ ksi (25.2 MN/m²); $R = 0.05$.

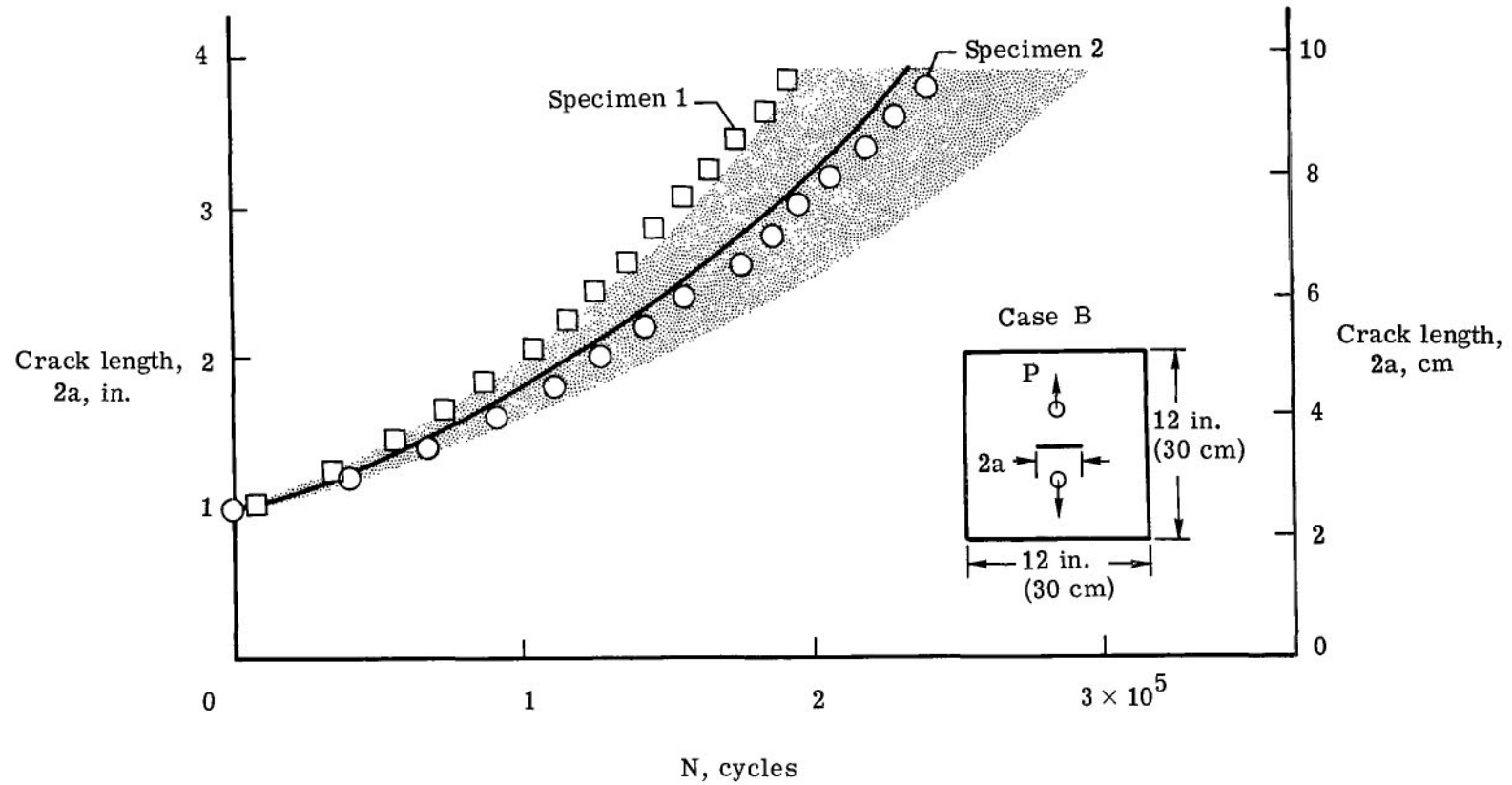


Figure 3.- Comparison of predicted and experimental fatigue crack propagation for a symmetrically cracked 7075-T6 aluminum-alloy panel subjected to concentrated forces. $P_{\max} = 1920 \text{ lbf}$ (8.55 kN); $R = 0.05$.

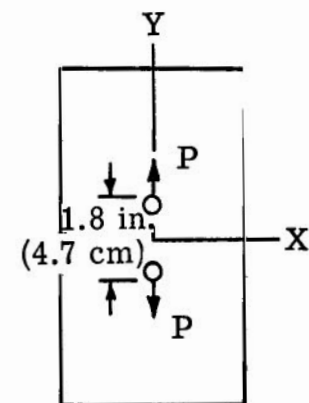
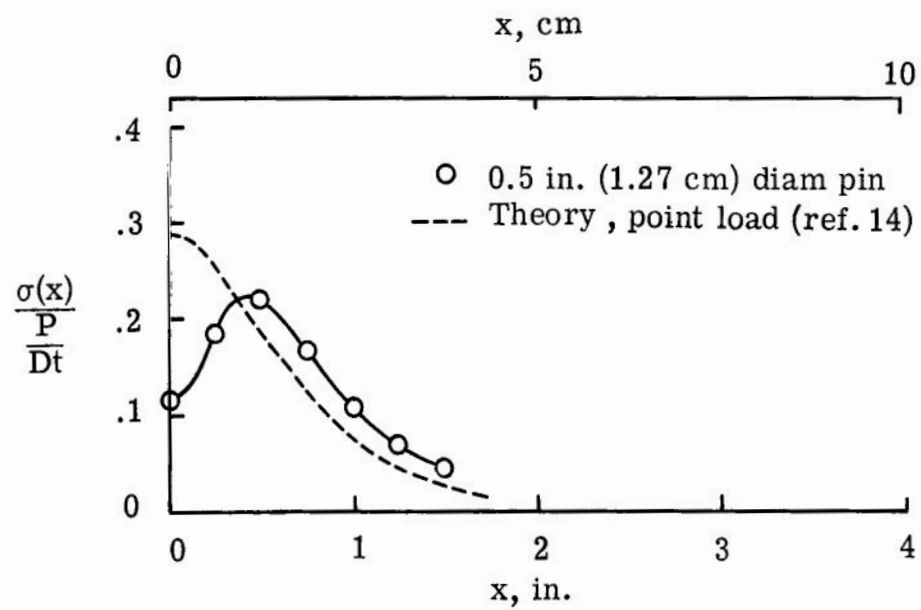


Figure 4.- Theoretical stress distribution at $y = 0$ for point loads and measured stress distribution for loads applied through pins.
 $t = 0.091$ inch (0.23 centimeter).

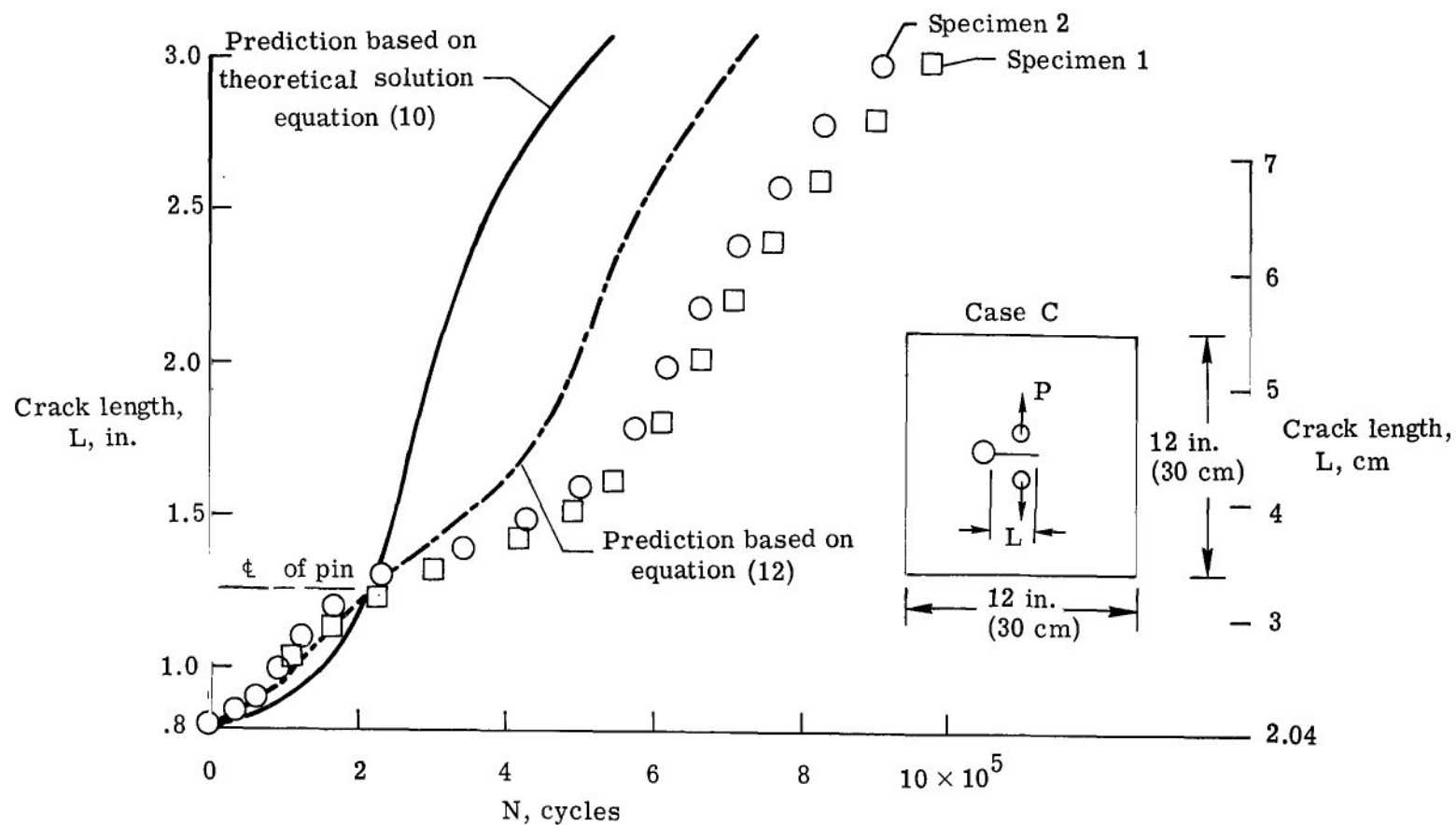


Figure 5.- Comparison of predicted and experimental fatigue crack propagation from one side of a hole located eccentrically in a 7075-T6 aluminum-alloy panel subjected to concentrated forces. $P_{\max} = 1150$ lbf (5.12 kN); $R = 0.05$.

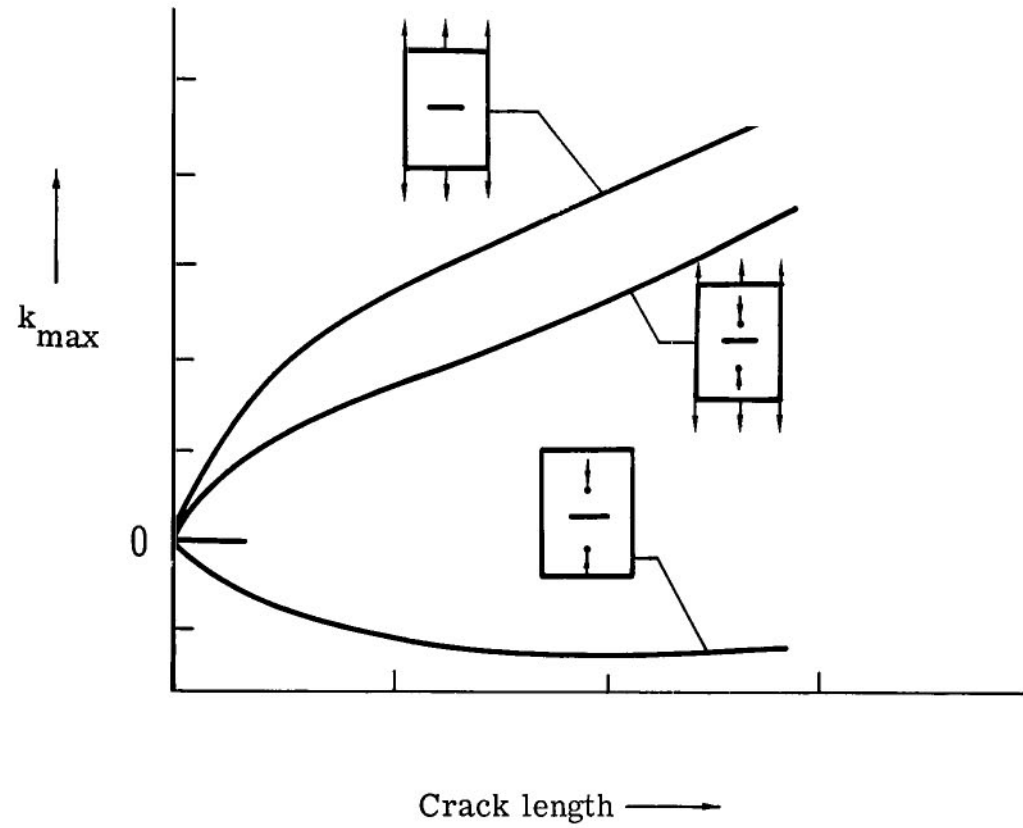


Figure 6.- Superposition method to obtain stress-intensity factors for a symmetrically cracked panel subjected to concentrated compression forces.

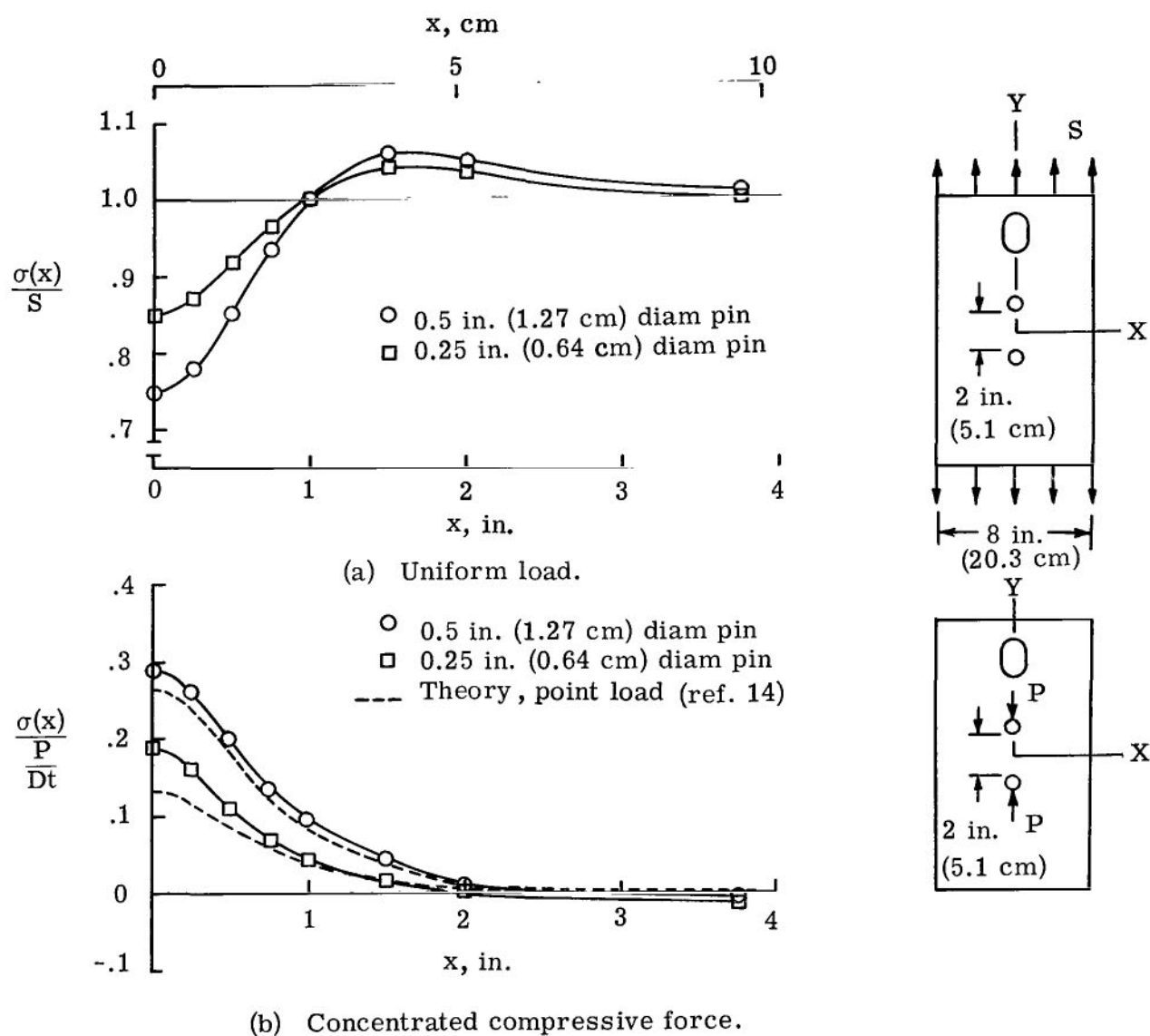
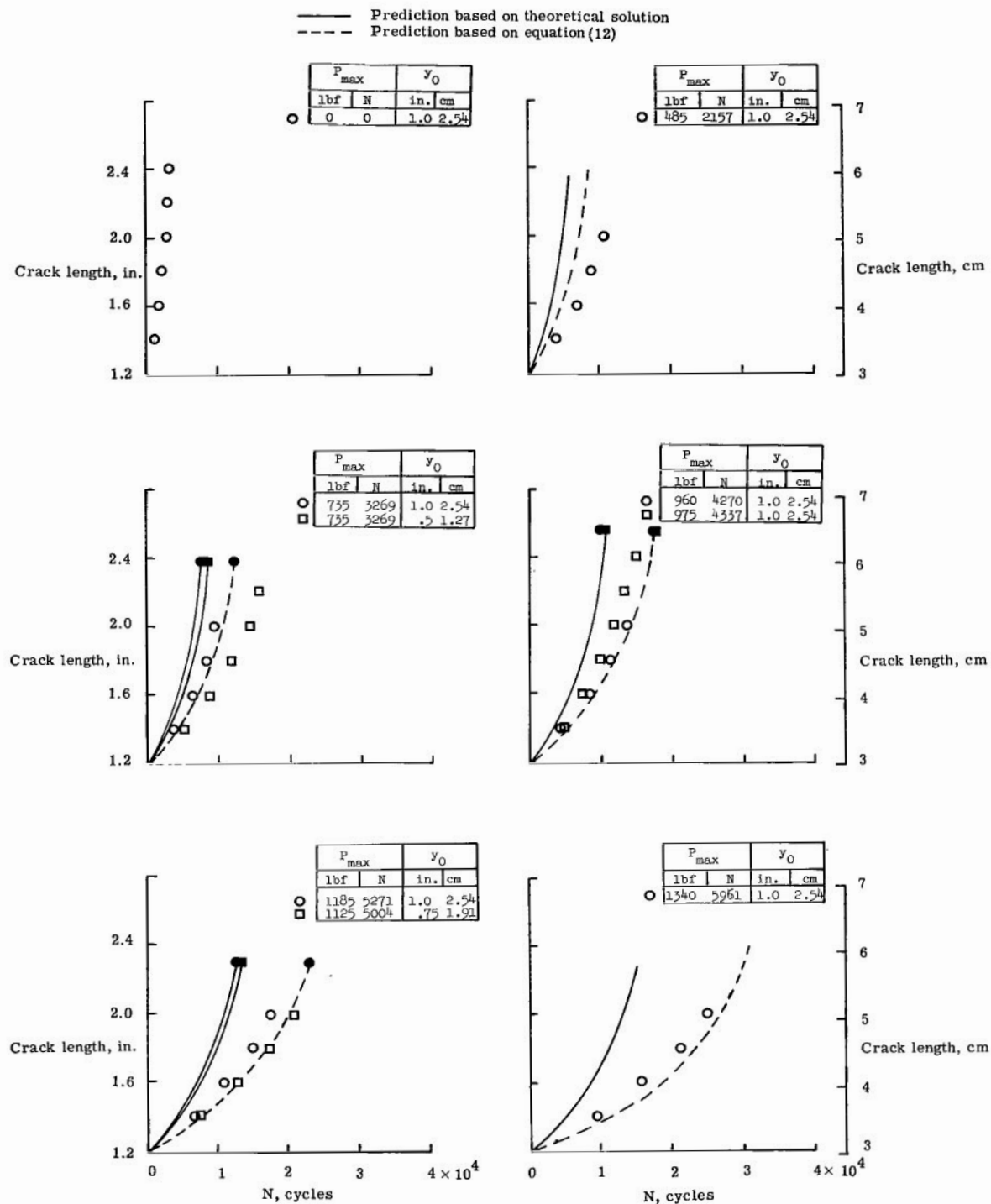
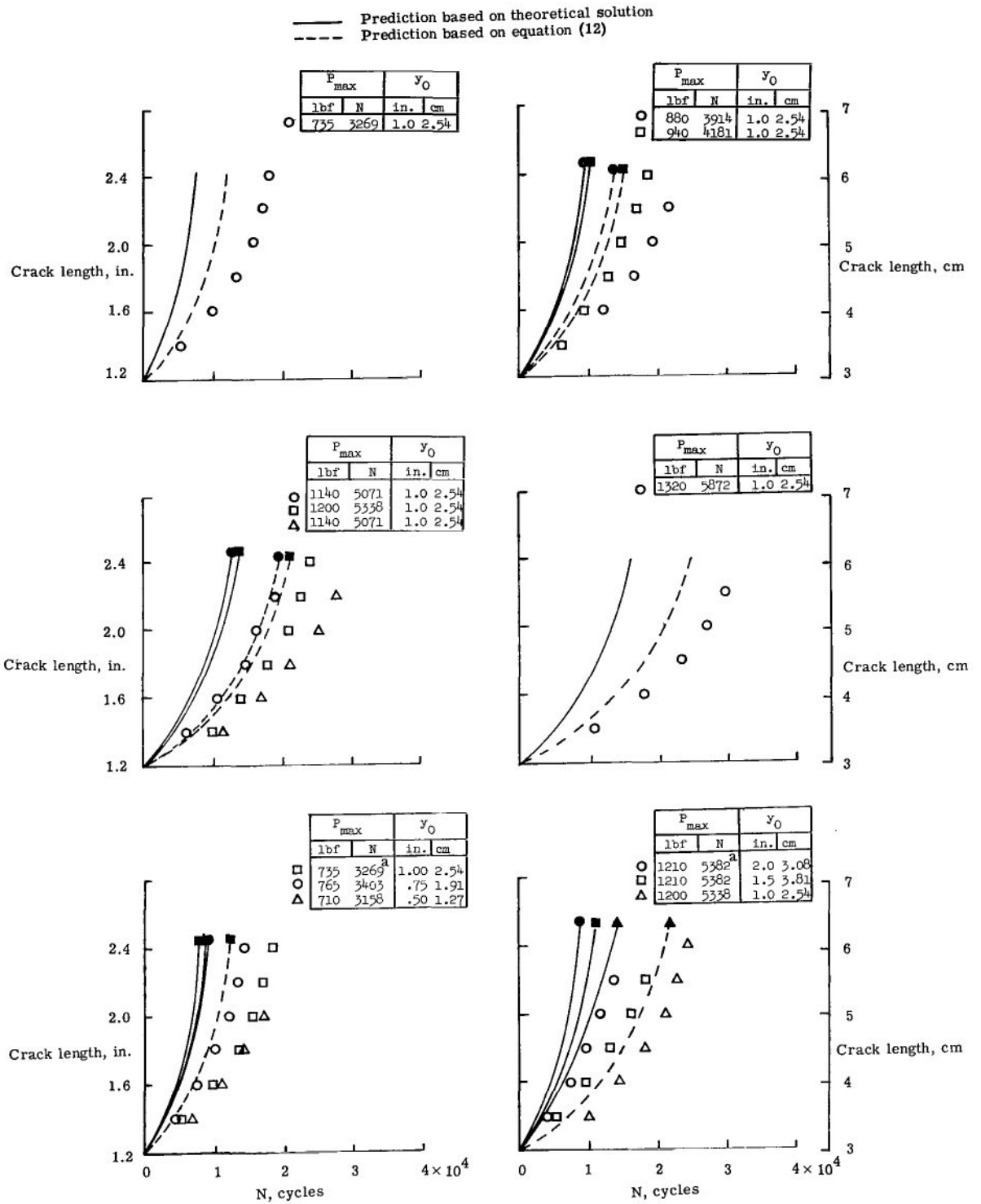


Figure 7.- Comparison of stress distributions at $y = 0$ in panels subjected to uniform loads or to pin loads. $t = 0.091$ inch (0.23 centimeter).



(a) Pin diameter 0.25 in. (0.64 cm); $S_{max} = 14.8$ ksi (102.0 MN/m²); 7075-T6 aluminum alloy.

Figure 8.- Measured and predicted crack length against cycles for case D. The solid symbols represent the predicted results for the corresponding experimental data (open symbol).



(b) Pin diameter 0.50 in. (1.27 cm); $S_{max} = 14.8$ ksi (102.0 MN/m²); 7075-T6 aluminum alloy. Footnote a in tables denotes data used more than once in comparisons.

Figure 8.- Concluded.

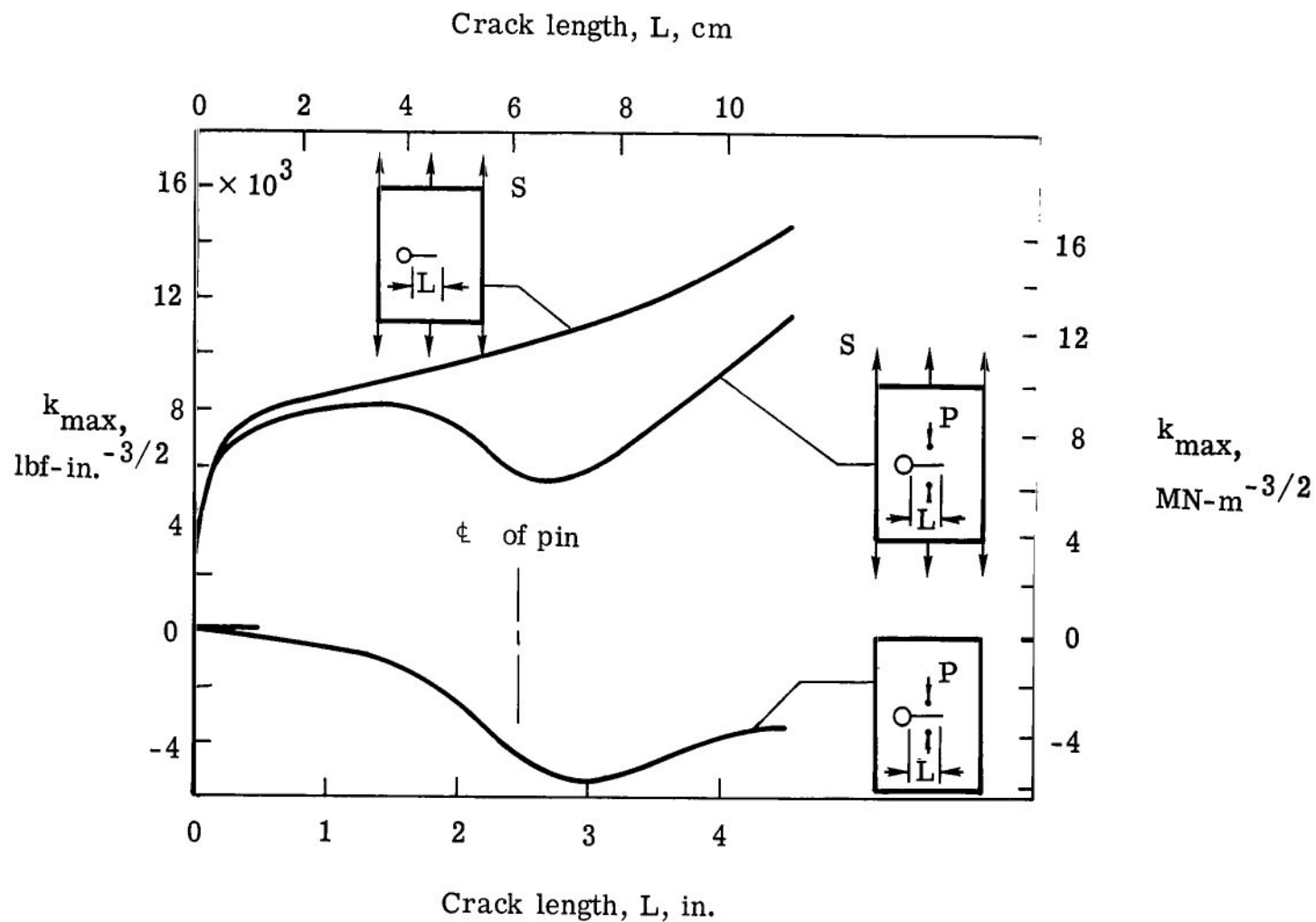


Figure 9.- Superposition method for stress-intensity factors for a fatigue crack growing from one side of a hole located eccentrically in a 7075-T6 aluminum-alloy panel subjected to concentrated compression forces. $S_{\max} = 8$ ksi (55 MN/m²); $R = 0.05$; $P_{\max} = 1090$ lbf (4.85 kN); $P_{\min} = 910$ lbf (4.05 kN).

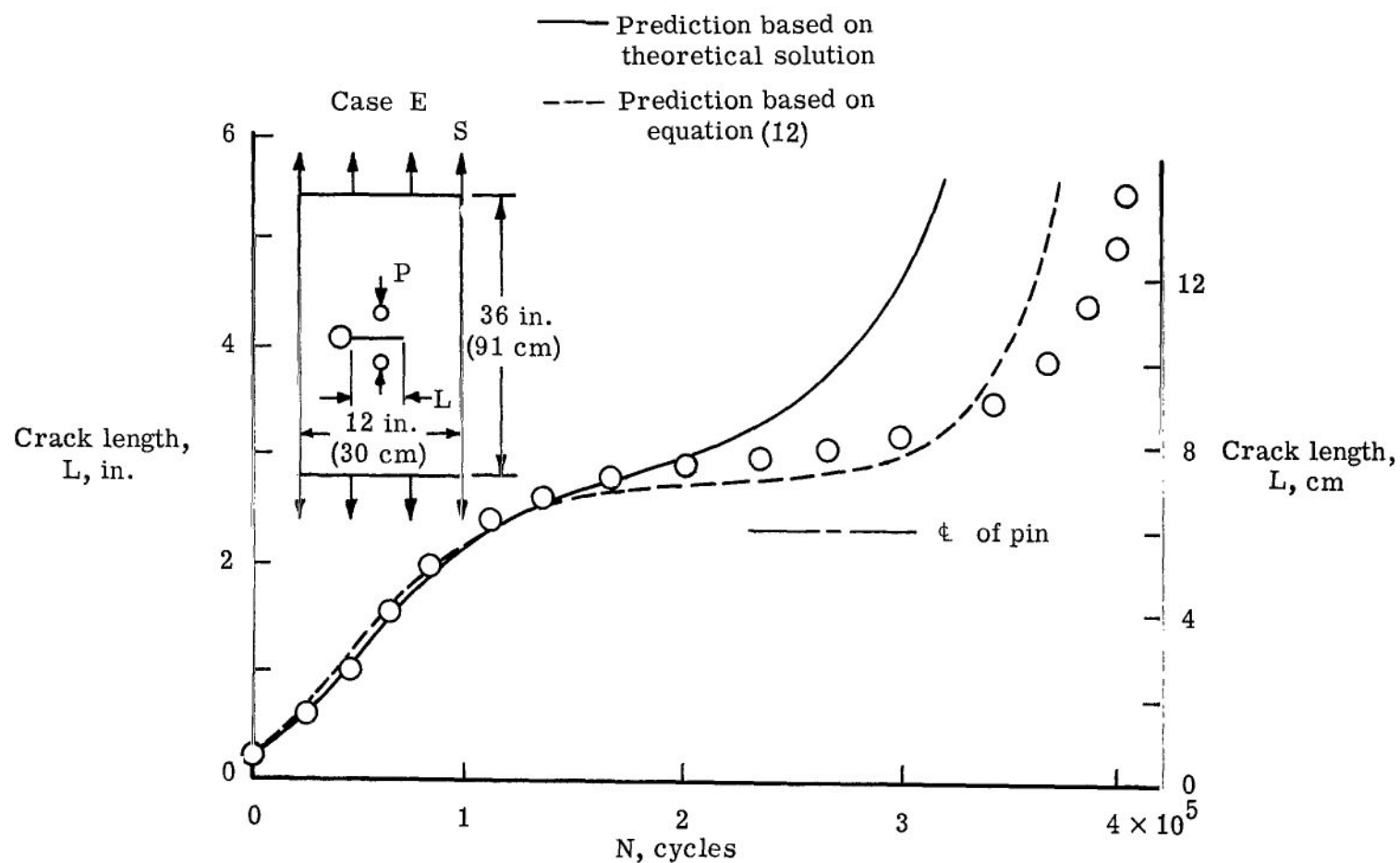


Figure 10.- Fatigue crack propagation from one side of a hole located eccentrically in a 7075-T6 aluminum-alloy panel subjected to uniform load and concentrated forces. $S_{\max} = 8$ ksi (55 MN/m²); $R = 0.05$; $P_{\max} = 1090$ lbf (4.85 kN); $P_{\min} = 910$ lbf (4.05 kN).

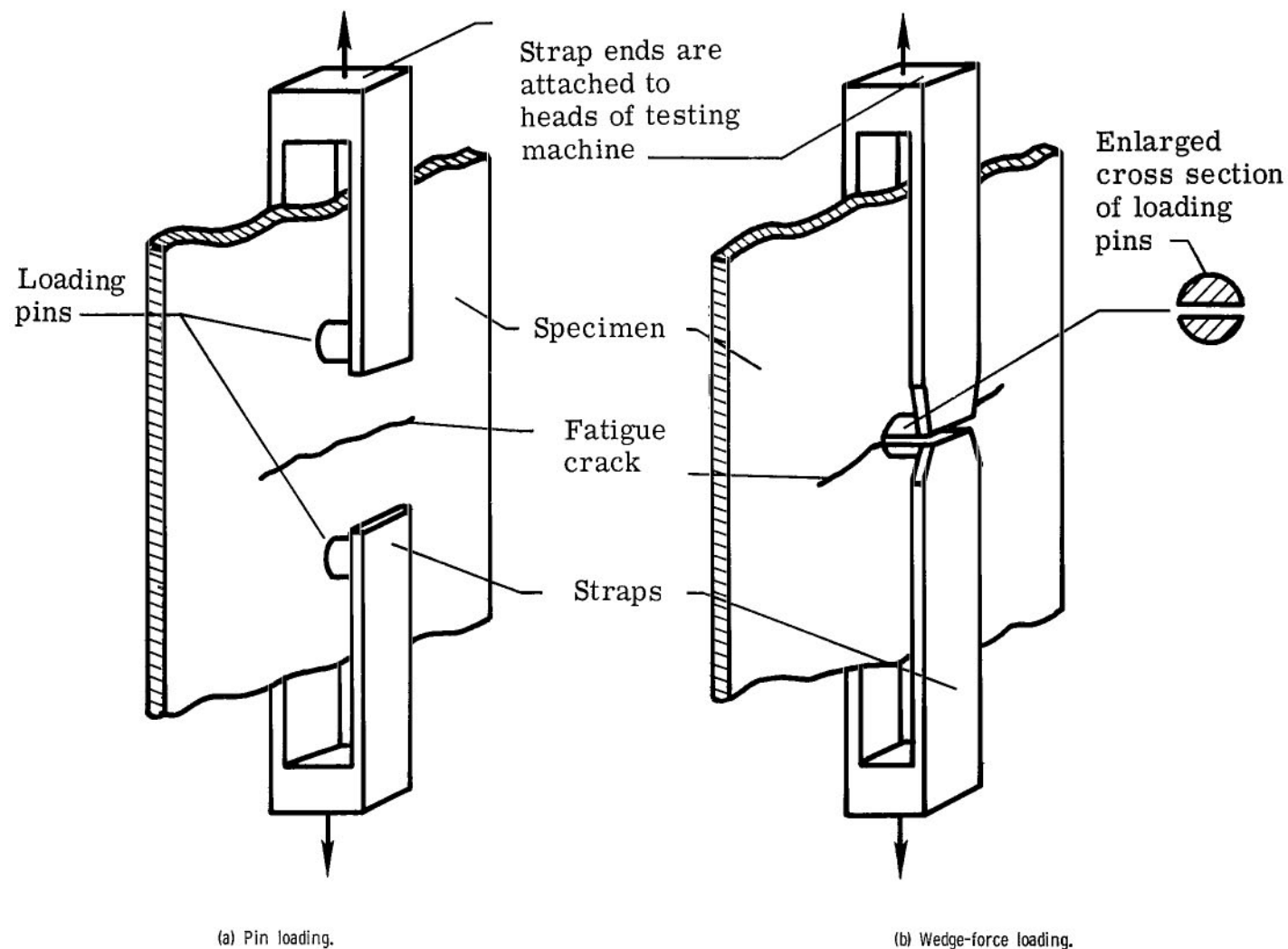


Figure 11.- Fixtures used to apply concentrated cyclic tension forces.

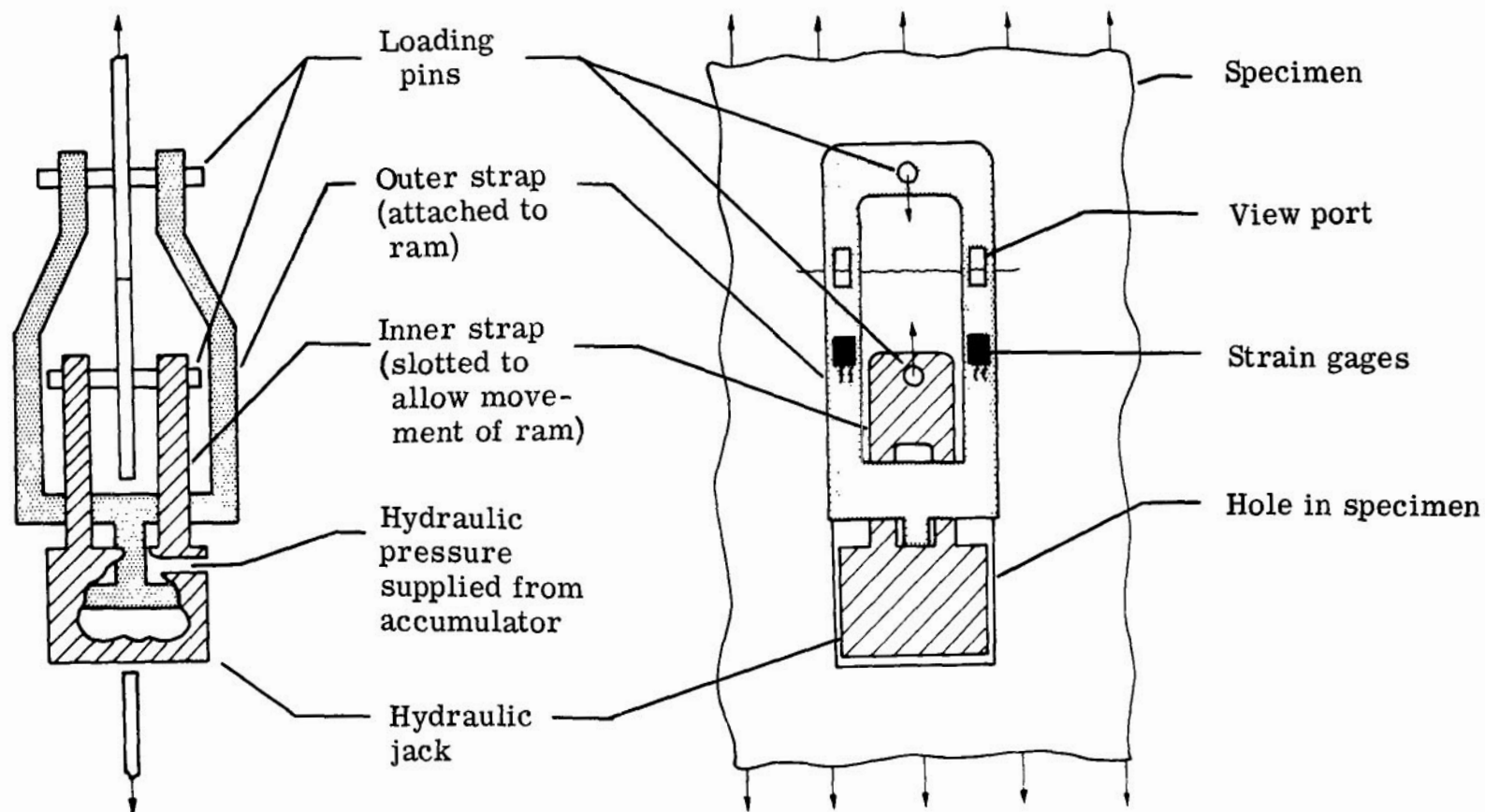


Figure 12.- Schematic of fixture used to apply static concentrated compression forces.

FIRST CLASS MAIL

1 57 51 822 6 00903
1 57 51 822 6 00903
1 57 51 822 6 00903

POSTMASTER: If Undeliverable (Section 15
Postal Manual) Do Not Return

"The aeronautical and space activities of the United States shall be conducted so as to contribute . . . to the expansion of human knowledge of phenomena in the atmosphere and space. The Administration shall provide for the widest practicable and appropriate dissemination of information concerning its activities and the results thereof."

— NATIONAL AERONAUTICS AND SPACE ACT OF 1958

NASA SCIENTIFIC AND TECHNICAL PUBLICATIONS

TECHNICAL REPORTS: Scientific and technical information considered important, complete, and a lasting contribution to existing knowledge.

TECHNICAL NOTES: Information less broad in scope but nevertheless of importance as a contribution to existing knowledge.

TECHNICAL MEMORANDUMS: Information receiving limited distribution because of preliminary data, security classification, or other reasons.

CONTRACTOR REPORTS: Scientific and technical information generated under a NASA contract or grant and considered an important contribution to existing knowledge.

TECHNICAL TRANSLATIONS: Information published in a foreign language considered to merit NASA distribution in English.

SPECIAL PUBLICATIONS: Information derived from or of value to NASA activities. Publications include conference proceedings, monographs, data compilations, handbooks, sourcebooks, and special bibliographies.

TECHNOLOGY UTILIZATION PUBLICATIONS: Information on technology used by NASA that may be of particular interest in commercial and other non-aerospace applications. Publications include Tech Briefs, Technology Utilization Reports and Notes, and Technology Surveys.

Details on the availability of these publications may be obtained from:

SCIENTIFIC AND TECHNICAL INFORMATION DIVISION
NATIONAL AERONAUTICS AND SPACE ADMINISTRATION
Washington, D.C. 20546